EXCELLENT PUBLISHERS

International Journal of Current Research and Academic Review

ISSN: 2347-3215 Volume 3 Number 7 (July-2015) pp. 63-90

www.ijcrar.com

Quantum chemical investigation on the conformers of 2-hydroxybenzamide with emphasize on hydrogen bonding

V. Krishnakumar[1], K.Mangaiarkkarasi[2]* and N.Surumbarkuzhali[2]

[1]Department of Physics, Periyar University, Salem-636011, India
[2]Departmentof Physics, Government Arts College (Autonomous), Salem - 636007, India

Corresponding author

KEYWORDS

Quantum chemical, 2-hydroxybenzamide, Density functional theory (DFT) methods

A B S T R A C T

The ground state conformational properties of the monomer and the dimer of 2-hydroxybenzamide (2HBA) have been investigated using density functional theory (DFT) methods using the B3LYP/6-31G** basis set. DFT calculations predict the ground-state geometries in quantitative agreement with the available experimental results. This also indicates that H-bond interaction plays an important role in the conformational energy and harmonic vibrational frequencies in biological molecules. The DFT predicted wavelengths are comparable to the experimentally observed FT-IR and FT-Raman spectra. In addition, DFT calculations predict qualitatively correctly the red shift transition in hydrogen bonded conformer. Geometrical parameters, natural bond orbital analysis and molecular electrostatic potential maps of conformers have been discussed to explore the hydrogen bonds among them. The stabilization energies E(2) have been calculated by natural bond (NBO) analysis to give clear evidence of stabilization originating in the hyper conjugation of hydrogen–bonded interactions. The harmonic vibrational frequencies were calculated and the scaled values have been compared with experimental FT-IR and FT-Raman spectra. The observed and the calculated frequencies are found to be in good agreement. The electronic properties, such as HOMO and LUMO energies, were performed by DFT approach.

Introduction

Benzamide is an off-white solid. Since it is a derivative of benzoic acid, they are essential components of the vitamin B-complex (Sundaraganesan *et al.*, 2008). The derivatives of amide and its hydrolysis reaction are concentrated for quite a long time due to its biological importance. Salicylamide is the common name for the substance 2-hydroxybenzamide (2HBA), or amide of salicyl. Salicylamide is an important fine chemical intermediate, which has versatile applications in the production of dyes, pigments, pharmaceuticals and spicery.

Salicylamide is also a non-steroidal anti-inflammatory agent with analgesic and antipyretic properties. Its medicinal uses are similar to those of aspirin. Salicylamide is used in combination with both aspirin and caffeine in the over-the-counter pain remedies. Salicylamide is a pain reliever. It is used to relieve mild to moderate pain from headaches, the common cold, flu, or a sinus infection (Sullivan and Sherma, 2006). It may also be

used for pain from menstrual cramps, muscle or nerve pain, and arthritis. It works by blocking substances in the body that cause fever, pain, and inflammation. Salicylamide is a salicylic acid derivative but is not hydrolyzed to salicylate; it is almost completely metabolized to inactive metabolites during absorption and on first pass through the liver. Salicylamide has also been applied topically in various preparations in concentrations of up to 8.5% for the relief of muscular and rheumatic pain. It has been used in protections against fungus in, for example, oils, soaps, and lotions. However, the molecular structure of 2HBA is quite fascinating for conformational analysis.

Yifan Jin *et al.* studied the Theoretical analysis on alkaline hydrolysis mechanisms of N-(2-methoxyphenyl) benzamide (Yifan Jin *et al.*, 2011). Arjunan *et al.* (2011) studied the Experimental and theoretical investigations of benzamideoxime. X ray diffraction data of 5-chloro-2-hydroxy-benzamide, 2-Hydroxy-N,N-diethyl-benzamide has been reported by P. Kawski *et al.* (2006). Gas phase diffraction of benzamide was analyzed by Konaka *et al.* (1999). To the best of our knowledge, neither hydrogen bonding, nor the conformational analysis of 2-hydroxybenzamide (2HBA) have been reported, as yet. Therefore, with all these in consideration, we set our goal to examine conformers of this compound completely and to identify type and strength of hydrogen bonding in detail.

Hydrogen bonding has been one of the most interesting areas of research mainly due to its vital role in many chemical and biological processes. During the past few decades, a large number of experimental and theoretical studies have been devoted to the elucidation of structures where intra- and intermolecular hydrogen bonding plays a crucial role in determining the stability of the molecular systems (Cotton and Luck, 1989; Zeegers *et al.*, 1991). The hydrogen bonds are conventionally shown as A-H…B where the H atom is shared between A and B atoms. Usually A is an electronegative atom and B is either an electronegative atom having one or more lone electron pairs or a region of excess electron density such as aromatic systems. In a normal hydrogen bond, there is significant charge transfer from the proton acceptor B to the proton donor (A-H), resulting in a weakening of the A-H bond leading to bond elongation and a consequent decrease of the A-H stretching vibration frequency. This red shift in A-H stretching vibration, which is often of the order of several tens of wave numbers, is usually considered to be the most important and easily detectable manifestation of the formation of an H-bond, even in an O-H…O system (George Socrates, 2001). Hence, we analyze the conformers of title molecule in the light of hydrogen bonding with the aid of NBO and MEP computations. The density functional theory (DFT) calculations have been performed to support our wave number assignments.

Experimental details

The compound under investigation namely 2HBAwere kindly provided by the Sigma chemical company (U.S.A) and used as such for the spectral measurements. The room temperature Fourier transform infrared spectra of the title compounds are measured with KBr pellet technique in the 4000-400 cm^{-1} region at a resolution of ±1 cm^{-1} using BRUKER IFS 66V FTIR spectrometer equipped with a cooled MCT detector for the mid-IR range. Boxcar apodization is used for the 250 averaged interferograms collected for the sample and background.

Computational details

The combination of spectroscopic methods with DFT calculations are powerful tools for understanding the fundamental vibrational properties and the electronic structure of the compounds. The Ab initio calculations, full geometry optimization and calculation of the harmonic vibrational frequencies were performed using the GAUSSIAN 09W program (Frisch *et al.*, 2009), within the Density Functional Theory (DFT) approach, in order to properly account for the electron correlation effects (particularly important in this kind of

conjugated systems). The widely employed hybrid method denoted by B3LYP, which includes a mixture of HF and DFT exchange terms and the gradient-corrected correlation functional of Lee, Yang and Parr, as proposed and parameterized by Becke (1993) and Lee *et al.* (1988) was used, along with the double-zeta split valence basis set 6-31G** (Becke, 1988; Foresman and Frisch, 1996).

Molecular geometries (of both monomeric and dimeric species) were fully optimized by the Berny algorithm (Schlegel, 1982), using redundant internal coordinates. No geometrical constraints were imposed on the molecules under study. All frequency calculations were run at the B3LYP/6-31G** level and wavenumbers above 400 cm^{-1} were scaled before comparing them with the experimental data. Harmonic frequency calculations were performed for all the optimized structures to establish that the stationary points are minima. The vibrational characterization was based on the normal-mode analysis performed according to the Wilson FG matrix method using standard internal coordinates and the scaling factors of Rauhut and Pulay (1995) (Fogarasi and Pulay, 1985; Fogarasi *et al.*, 1992; Pulay *et al.*, 1983).

The shapes of molecules can be predicted by tallying up estimates of steric and torsional interactions. This task is referred to as function optimization, which is a calculation that pervades much of numerical analysis. In the context of molecules, the function to be optimized (minimized) is energy. The energy landscape of a molecule may possess an enormous number of minima, or conformational substrates. Nonetheless, the goal of energy minimization is simply to find the local energy minimum, i.e., the bottom of the energy well occupied by the initial conformation. The energy at this local minimum may be much higher than the energy of the global minimum. Physically, energy minimization corresponds to an instantaneous freezing of the system; a static structure in which no atom feels a net force corresponds to a temperature of 0 K. In optimizing any molecule, the computation may reach the position of a particular conformation which occupies a "local energy minimum", meaning that the energy is lower here than when the dihedral angle is either greater or smaller, because in either direction the molecule would arrive at an eclipsed conformation with higher energy.

In the approach described above, typically the default approach in most calculations, the computer could get stuck at the particular conformation, because a change in either direction results in an increase in energy. However, if the computer would just push past those energy maxima then it would arrive at the anti conformation, which is the "global energy minimum", with the lowest energy of all. Complete conformational analysis sometimes requires some method of "dihedral angle driving", which we adopted in the present investigation. The structure of the title compound shown in Fig. 1 is very flexible.

It has got four conformations (Figs. 1A to 1D). To establish the most stable conformation as the initial point for further calculations, the molecule was submitted to a rigorous conformation analysis around the free rotation bonds. The impact of intra and inter molecular hydrogen bonding in 2HBA was our main object of study in this paper.

Table 1 comprises the optimized energies at the B3LYP/6-31G** level for the conformers of 2HBA. Table 1 and figure 2 show that the Conformer in figure 1(A) is the most stable. Therefore, further in this paper, we focus on this particular form of the title compound. The structure corresponding to global minimum energy value has been taken for NBO analysis. The study shows, there is redistribution of electron density showing intra molecular hydrogen bonding between $O_8$of carbonyl group and H_{13} of hydroxyl group as depicted in figure 3. The literature survey reveals that the spectra of carbonylatoms exhibit a broad band due to the O-H and N-H stretching vibrations and a strong band due to the C=O stretching vibration in the dimer environment which will possess strong inter and intra molecular

hydrogen bonding among the molecule (Karabacak Mehmet and Kurt Mustafa, 2009). So, further analysis is needed for exploring the molecular structure, as the experimental IR peaks of amino, hydroxyl and carbonyl group illustrate the occurrence of strong hydrogen bonds. The computation then extended for dimer structure. The NBO analysis of dimer structure substantiates strong inter molecular interaction between O_8 of one molecule with H_{27} of another molecule and O_{25} of one molecule with H_{10} of another molecule as in Fig. 3. These hydrogen bridges are responsible for cyclic dimer structure of 2HBA. The structures of monomer and dimer have been taken for molecular electrostatic potential calculation also. These results confirm the existence of inter molecular hydrogen bonds formed between adjacent molecules of 2HBA and intra molecular hydrogen bonding between carbonyl and hydroxyl groups.

The Cartesian representation of the theoretical force constants have been computed at optimized geometry by assuming C_s point group symmetry. The theoretical DFT force field was transformed from Cartesian into local internal coordinates and then scaled empirically according to the SQM procedure (Lee *et al.*, 1988; Becke, 1993; Forsyth and Sebag, 1997).

$$\mathbf{F_{ij}^{scaled} = (C_iC_j)^{1/2}\ F_{ij}^{B3LYP}} \quad \ldots (1)$$

Where $\mathbf{C_i}$ is the scale factor of coordinate **i**, $\mathbf{F_{ij}^{B3LYP}}$ was the B3LYP/6-31G** force constant in the local internal coordinates, and $\mathbf{F_{ij}^{scaled}}$ was the scaled force constant. Multiple scaling of the force field has been performed by the SQM procedure (Rauhut and Pulay, 1995; Pulay *et al.*, 1983) to offset the systematic errors caused by basis set incompleteness, neglect of electron correlation and vibrational anharmonicity (Foresman and Frisch, 1996). Scaling of the force field was performed according to the SQM procedure (Fogarasi and Pulay, 1985; Fogarasi *et al.*, 1992) using selective scaling in the natural internal coordinate representation (Rauhut and Pulay, 1995; Pulay *et al.*, 1983). Transformations of the force field and the subsequent normal coordinate analysis including the least square refinement of the scaling factors, calculation of the total energy distribution (TED) and the prediction of IR and Raman intensities were done on a PC with the MOLVIB program (version 7.0–G77) written by Sundius (Forsyth, and Sebag, 1997; Sundius, 1990). For the plots of simulated IR and Raman spectra, pure Lorentzian band shapes were used with a band width (FWHM) of 10 cm^{-1}. The force field obtained by this way was then used to recalculate the normal modes, TED's and the corresponding theoretically expected IR and Raman intensities to predict the full IR and Raman spectra. For the plots of simulated IR and Raman spectra, pure Lorentzianband shapes are used with a band width (FWHM) of 10 cm^{-1}. The Raman activities (Si) calculated by GAUSSIAN 09W program have been suitably adjusted by the scaling procedure with MOLVIB and subsequently converted to relative Raman intensities (Ii) using the following relationship derived from the basic theory of Raman scattering (Pulay *et al.*, 1983; Rauhut and Pulay, 1995; Foresman and Frisch, 1996).

$$I_i = \frac{f(\upsilon_0 - \upsilon_i)^4 S_i}{\upsilon_i\left[1 - exp\left(\frac{-hc\upsilon_i}{kT}\right)\right]} \ldots\ldots\ldots\ldots\ldots\ldots\ldots\ldots\ldots\ldots\ldots\ldots\ldots\ldots (2)$$

Where υ_0 is the exciting wave number (in cm^{-1} units), υ_i the vibrational wave number of the i^{th} normal mode, h, c, and k were the universal constants and f was a suitably chosen common normalization factor for all peak intensities.

Results and Discussion

Conformational Properties

2HBA has two main rotation axes (C_1-C_7 and C_2-O_{12} bonds) that give rise to 4 conformational isomers. The relevant torsion angles can be specified as $\tau_1(O_8\text{-}C_7\text{-}C_1\text{-}C_2)$and $\tau_2(H_{13}\text{-}O_{12}\text{-}C_2\text{-}C_1)$. Schematically, the central part of the molecule is kept frozen and each lateral unit is allowed to turn upon it in two different ways with the dihedral angles as 0° and 180° which leads to 4 conformers. On the

basis of a careful analysis of the potential energy map of 2HBA and preliminary energy optimizations, it is confirmed that the most stable structure belongs to the conformer A. Common to all DFT optimized conformers is that their molecular shape resembles an approximately planar sheet showing C_s symmetry, except for the conformer C, which deviates from planar structure due to the steric repulsion existing between hydrogen atoms of amide and hydroxyl groups and yields an unstable structure with imaginary frequencies. So, hereafter we are concentrating on the other three forms of conformer of 2HBA with stable structures. On investigating the structures, the conformer A and D seems to possess intra molecular hydrogen bonding. The position of H-Bridge depends on the molecular orientation i.e., in the conformer A the H-bonding is expected to form between O_8 of amide moiety and H_{13} of hydroxyl group and in D between O_{12} of hydroxyl group and H_{11} of amino moiety in amide functional group. So, we inspected the conformers with further studies like NBO and MEP that will throw light on the strength of hydrogen bonding and reason out the molecular circumstances that favour the conformer A as the most stable one.

Investigation of hydrogen bonding

Hydrogen bonding is clearly a major factor controlling the structure of molecules such as DNA and proteins. The optimized structures of 2HBA obtained at the B3LYP/6-31G** level are shown in figures 1(A) to 1(D). All structures exhibit C_1 symmetry with the nearly planar structure. It must be pointed out that the geometry with this symmetry and the structure with adjacent electropositive and electronegative moieties can form intramolecular hydrogen bonding. The existence of inter or intra molecular hydrogen bonding in a molecular circumstances can be interpreted in the following ways.

i) Analysis of geometrical parameters
ii) Spectroscopic study
iii) Natural bond orbital analysis
iv) Molecular Electrostatic Potential (MEP) maps

All the studies have been attempted for the chosen molecule. The detailed analyses illustrate the strength of intra molecular interaction.

Analysis of geometrical parameters

The geometrical bond lengths optimized at the B3LYP/6-31G** level for all conformers are listed in table 2. On comparing the bond lengths of hydroxyl group and carbonyl group in molecular structures of conformers, we have seen that the conformer A exhibited appreciable elongation in the bond lengths of hydroxyl group and carbonyl group. Approximately, the elongations are 1.246Å and 0.995 Å for carbonyl group and hydroxyl group respectively. The elongation of bonds always accounts for the formation of hydrogen bridge (Sathyanarayana, 1996; Karabacak Mehmet and Kurt Mustafa, 2009), longer the bond stronger the intra molecular attraction. Similarly, shortening of C_1-$C_7$and C_2-O_{12}in the conformer A, is also noticed which also interpret the existence of hydrogen bonding (Karabacak Mehmet and Kurt Mustafa, 2009). Inspecting the bond lengths of amino moiety surprising results have been observed. i.e., the bond distance of N_9-H_{10} (1.01Å) is longer than N_9-H_{11}(1.006 Å). Examination of similar structures like 5-chloro-2-hydroxybenzamide and benzamideshows the possibility of occurrence of intermolecular hydrogen bonding (Kawski *et al.*, 2006). Normally, the intra and inter molecular attractions alter geometry of amino, carbonyl and hydroxyl moiety due to hydrogen bonding. Hence the dimer structure is obtained through ab initio calculation.

The geometrical parameters of 2HBA for monomer and dimer structure are compared with available XRD data. Table 2 lists the bond distances of the conformers A, B and D including the gas phase XRD data taken from (Takeuchi *et al.*, 1996) and the mean deviation of bond distances of monomer and dimer from XRD data. As told earlier, the conformer A shows more elongation than conformer D for intra molecular bonds (C_7-O_8 = 1.246Å, O_{12}-H_{13}= 0.996Å). Despite the intra molecular

attraction, the structure A also shows inter molecular bonding of $H_{10}$with the O_8 of another molecule. The corresponding bond distances of N_9-H_{10}(1.01Å) and C_7-O_8(1.246Å) are much longer in conformer A. The existence of both kinds of H-bridge in the molecular environment accounts for the global minimum energy possessed by the conformer A than the other conformers. The computationally predicted bond lengths of conformer A as monomer coincide well with computationally predicted bond lengths of dimer as well as with XRD data. The minimum mean deviations from experimental data substantiate the fact of hydrogen bonding, as the experiment parameters are obtained from the dimer structure.

The computationally predicted endocyclic angles such as C_6-C_1-C_2, C_1-C_2-C_3, C_2-C_3-C_4, C_4-C_5-C_6 and C_5-C_6-C_1 are listed in Table 3. All the endocyclic angles of conformer A are computed as approximately 120°except for C_2-C_1-C_6 whereas the conformers B and D show deviations from 120° for the angles C_2-C_1-C_6, C_2-C_3-C_4 and C_5-C_6-C_1. This deviation is due to inductive effect offered by substitution of functional group of amide. The conformer A show reduced inductive effect of amide group than the conformers B and D, as the enhanced inter and intra molecular attractions of conformer. A reduces the electro negativity of amide group compared to the conformer B and D. The reduction of inductive effect is noticed in the following order of conformers A>D>B. It is worth to mention that the conformer B which is free from hydrogen bond exhibit a dominating inductive effect. On comparing the valence angles of amide group and hydroxyl group in all the three conformers, it is noticed that they are evident of hydrogen bonding. Generally an amide group has mixed hybridization of sp^2 and sp^3.

The conjugation of C_7 and N_9 nitrogen atoms give the preferredsp^2 hybridization, but it allows the rotation of H atoms about the CN bond which is essentially the sp^3 hybridization. It is obvious that electron donating and withdrawing nature of nitrogen (N_9) and oxygen (O_8) respectively are well reflected in the deformation angles (C_1-C_7-N_9~117°and C_1-C_7-O_8~123°) of conformer B. But, the hydrogen bonded conformers A (especially in dimer) and D are displaying approximately 120°, as they lack electronegative and electro positive character of oxygen and nitrogen atoms respectively due to hydrogen bonding. Typically the free hydroxyl group has exocyclic angles, as H-O-C~110° and O-C-C~120° (Muniappan *et al.,* 2014; Shobaa *et al.,* 2011), on contrary in the circumstance of hydrogen bonding, they are computationally predicted as 118° and 106° respectively, so as to favor the hydrogen bridge among hydroxyl and carbonyl moieties of conformer A and optimized values for the conformers B and D satisfies the condition of free hydroxyl groups. The deformations C_1-C_7-O_8, C_1-C_2-$O_{12}$and C_2-O_{12}-$H_{13}$for conformer A are computationally predicted as 121.8°, 118.0°and 106.0° respectively, whereas in dimer structure they have the values as120.1°,117.6° and 105.8^0.

The XRD data (Kawski *et al.,* 2006) coincides well with the deformations of dimer structure as it's predictions correspond to similar structure with hydrogen bond. The foresaid bond angles of other conformers are predicted in such a way that they exhibit prominent deviations from the XRD data. The hydrogen bonded distances are depicted in Fig.3.The hydrogen bonded distances $O_8 \ldots H_{13}$ = 1.63307 Å and $O_8 \ldots H_{27}$ = 1.86941 Åare much lesser than the sum of Van der Wall's radii (2.7 Å for O…H) in conformer A than the other conformers and strongly validate the presence of inter and intra molecular H-bridges.

Spectroscopic study

Spectral studies are, however based on geometrical parameters. The shift in geometrical parameters such as bond length, bond angle etc., alters the corresponding vibrational frequencies. The observed FT-IR and FT-Raman spectra are presented with the computationally predicted spectra in Figs. 4 and 5. The experimental FT-IR spectrum in figure 4 shows bands of O-H and N-H

stretching vibrations which is of medium to strong intensity with weak C-H stretching bands superimposed on it and the spectral region for those vibrations is shifted to lower wave numbers. Literature study shows, in general, intermolecular hydrogen bonded aminoand hydroxyl groups exhibit a strong band with bands due to C-H stretching vibrations in the region of 3100–2800 cm^{-1} to George Socrates (2001) (Sathyanarayana, 1996).

The above fact is in excellent consistent with the experimentally obtained results. Generally the carbonyl group stretching vibration become the finger print of it's substituted compounds. In the present circumstance, it was greatly affected and made its appearance at 1674 cm^{-1} in FT-IR spectra. As there is intermolecular hydrogen bond existing among carbonyl group and hydroxyl group, the double bond character of carbonyl group is decreased. It makes the force constant to recede which results in a lowering of wave number. The corresponding bond lengths are increased (George Socrates, 2001). All these criterions are clearly noticeable in the present study and confirm the existences of strong inter and intra molecular hydrogen bonding in the 2HBA. The occurrence of intra and inter molecular hydrogen bonding makes the respective hydroxyl and amino bands to appear in the lower wavenumber region of 3300 to 3000cm^{-1}.

Natural Bond Orbital Analysis

Natural bond orbital analysis provides an efficient method for studying intra- and inter-molecular bonding and interaction among bonds and also provides a convenient basis for investigating charge transfer or conjugative interaction in molecular systems. NBO analysis has been performed on the monomer and dimer structure of the molecule at the DFT/B3LYP/6-31G** level in order to elucidate the intermolecular rehybridization and delocalization of electron density within the molecule. The second-order Fock matrix has been carried out to evaluate the donor–acceptor interactions in the NBO basis (Reed *et al.*, 1988). The interactions result in a loss of occupancy from the localized NBO of the idealized Lewis structure into an empty non-Lewis orbital. For each donor (i) and acceptor (j), the stabilization energy E(2) associated with the delocalization i→j is estimated as

$$E(2) = \Delta E_{ij} = q_i \frac{F(i,j)^2}{\varepsilon_i - \varepsilon_j} \quad \ldots (3)$$

where, q_i is the donor orbital occupancy, $\varepsilon_i$and $\varepsilon_j$are diagonal elements and *F(i,j)* is the off diagonal NBO Fock matrix element (James *et al.*, 2006). Delocalization of electron density between occupied Lewis-type (bond or lone pair) NBO orbitals and formally unoccupied (antibond or Rydberg) non-Lewis NBO orbitals corresponds to a stabilizing donor–acceptor interaction. Some electron donor orbital, acceptor orbital and the interacting stabilization energy resulting from the second-order micro-disturbance theory are reported (Raschi and Romano, 2010; Szafran *et al.*, 2007). The larger the E(2) value, the more intensive is the interaction between electron donors and electron acceptors, i.e. the more donating tendency from electron donors to electron acceptors and the greater the extent of conjugation of the whole system (Ravikumar *et al.*, 2010).

The results of NBO analysis for monomer and dimer are compared. In the monomer analysis, there is an evidence for intra molecular hydrogen bonding between the atoms. The lone pair electrons of O_8 of carbonyl moiety and H_{13} of hydroxyl group involve in intra molecular interaction. This is well substantiated by the presence of stabilization energy from the oxygen atom (O_8) to the hydrogen atom (H_{13}). But, in dimer of 2HBA, the intermolecular interaction is formed by the orbital overlap of LP(O_8) with σ*(N_{26}─H_{27})bond orbital and also by O_{25}withσ*(N_9─H_{10})which results in the formation of cyclic dimer. These interactions are observed as increase in electron density (ED) in N_9─H_{10} and N_{26}─H_{27} antibonding orbitals and that weakens the respective bonds (ShrutiMaheshwary *et al.*, 2006) and causes their elongation. The stabilization energy E(2)

associated with hyperconjugative interactions $LP1(O_8)\rightarrow\sigma^*$ $(O_{12}\text{─}H_{13})$, $LP2(O_8)\rightarrow\sigma^*(O_{12}\text{─}H_{13})$, $LP1(O_8)\rightarrow\sigma^*(N_9\text{─}H_{10})$ and $LP2(O_8)\rightarrow\sigma^*$ $(N_9\text{─}H_{10})$ are obtained as 9.91, 23.77, 10.75 and 5.49 $kJmol^{-1}$ respectively (Table 5), which quantify the extend of strong intermolecular hydrogen bonding to form a cyclic dimer. These NBO results confirm that the electron delocalization is from the oxygen of the carbonyl group of first molecule to the hydrogen of amino group of another molecule and vice versa. Table 6 shows occupancies of bonding and antibonding orbitals that are involved in the intra and inter molecular attractions. Normally the occupancy of a bonding orbital has the value as 2. Loss of occupancy represents delocalization of that orbital. The delocalization of orbital is higher for atoms in hydrogen bonded conformers (A and D) than the non-hydrogen bonded one (B). On comparing the conformers A and D, delocalization is higher for the conformer A, which possess strong inter and intra molecular H-bridges.

The dimer structure obviously has highest delocalization.Table7 lists the changes in electron density in the lone pairs (O_8) and the antibonding (σ^*, π^*) NBOs during the formation of 2HBA dimer. The lone pair (O_8) and the antibonding orbital (σ^*) of C_1-C_7 show a large decrease in electron density that results in strengthening of the C_1-C_7 bond and hence the observed decrease in the bond distance (Table 2). There is also an increase in the electron density of the antibonding orbitalσ* of N-H. This weakens the N-H bond resulting in lengthening of the bond (ShrutiMaheshwary *et al.*, 2006). This result in bond elongation with concomitant red shift of stretching wave numbers of respective groups. That the changes in the bond distances are due to hydrogen bond formation is confirmed by natural bond orbital (NBO) analysis.

Molecular Electrostatic Potential

Electrostatic potential maps, also known as electrostatic potential energy maps, or molecular electrical potential surfaces, illustrate the charge distributions of molecules three dimensionally. These maps allow us to visualize variably charged regions of a molecule. Knowledge of the charge distributions can be used to determine how molecules interact with one another. It simultaneously displays the molecular shape, size, and charge distribution, as well as reactive sites of a molecule (Scrocco and Tomasi, 1978; Murray and Sen, 1996). The first step involved in creating an electrostatic potential map is collecting a very specific type of data: electrostatic potential energy. An advanced computer program calculates the electrostatic potential energy at a set distance from the nuclei of the molecule. Electrostatic potential energy is fundamentally a measure of the strength of the nearby charges, nuclei and electrons, at a particular position.

To accurately analyze the charge distribution of a molecule, a very large quantity of electrostatic potential energy values must be calculated. The best way to convey this data is to visually represent it, as in an electrostatic potential map. A computer program then imposes the calculated data onto an electron density model of the molecule derived from the Schrödinger equation. To make the electrostatic potential energy data easy to interpret, a colour spectrum, with red as the lowest electrostatic potential energy value and blue as the highest, is employed to convey the varying intensities of the electrostatic potential energy values.

The electrostatic potential is a physical property of a molecule related to how a molecule is first “seen” or “felt” by another approaching species. The MEP is a plot of the electrostatic potential mapped onto the constant electron density surface. The MEP maps allow us to visualize variably charged regions of a molecule in terms of colour grading. Areas of low potential, red (negative MEP) are characterized by an abundance of electrons or greatest electron density. A portion of a molecule that has a negative electrostatic potential is susceptible to electrophilic attack the more negative the better. Areas of high

potential, blue (positive MEP), are characterized by a relative absence of electrons. This area is the region of nucleophilic attack.

To predict reactive sites for electrophilic and nucleophilic attack for the investigated molecule in three of its conformations A, B and D, MEP studies were carried out by B3LYP using 6-31G** basis set. The negative (red and yellow) regions of the MEP are related to electrophilic reactivity and the positive (blue) regions to nucleophilic reactivity, as shown in figure 6 for monomer and dimer respectively. For monomer, as can be seen from the figure 6, negative region is mainly localized over the oxygen atoms (O_8) of the amide group and the oxygen atoms of hydroxyl groups (O_{13}). The maximum positive region is localized on the hydrogen atoms (H_{10} and H_{11}) of the amide group indicating a possible site for nucleophilic attack in conformer A. These sites give information about the region from where the compound can have intermolecular and intramolecular interactions. Thus, it would be predicted that the oxygen atom (O_8 and O_{12}) will be the most reactive site for electrophilic attack and hydrogen atoms (H_{10} and H_{11}) will be the reactive site for nucleophilic attack and enhancing dimer formation. This is also in support with the literature (Katritzky and Pozharski, 1979). At the same time Fig. 6, the MEP diagram of dimer clearly illustrates that the reactive sites for electrophilic and nucleophilic attacks lost their colour; because of donor-acceptor interaction exists among them. Similarly, the oxygen and hydrogen atoms (O_{12} and H_{13}) involved in the intramolecular interaction lost their colour. The conformer B, which has no hydrogen bonding shows rich colour contour for electro negativity of O_8 and O_{12} atoms comparatively, whereas conformer D displays colourless contours for atoms involving hydrogen bridge and colour enriched contours for other reactive sites for electrophilic attack and nucleophilic attack.

Molecular Geometry

The first task for the computational work is to determine the optimized geometry of the studied molecule in its most stable conformation. The geometry of the molecule under investigation is considered by possessing C_s point group symmetry. The symmetries of the vibrational modes were determined using the standard procedure (Rauhut and Pulay, 1995) of decomposing the traces of the symmetry operation into the irreducible representation. The 45 fundamental modes of vibrations of compound were distributed into the irreducible representations under C_s symmetry as Γ_{vib} = 31 in plane + 14 out of plane vibrations (Pulay *et al.,* 1983, 1979). All vibrations are active both in IR and Raman. All the frequencies are assigned in terms of fundamental, overtone and combination bands.

Structural properties

The computationally predicted bond lengths and bond angles of this compound in various conformations are listed in Table 2 and Table 3.The impact of inter and intra molecular interactions of title molecule is well reflected in its molecular structure especially in the functional group attachments, which can be depicted by analysing the geometrical parameters. Those interactions elongate the bond lengths of carbonyl group and hydroxyl group and alter the bond angles, which are explicitly explained in the Section 4.1. Optimized geometry shows that, structure of 2HBA is non-planar with the amide group dihedral angles viz., N_9–C_7–C_1–C_2, H_{10}–N_9–C_7–C_1, H_{11}–N_9–C_7–C_1 and O_8–C_7–C_1–C_2 of -173.5º, 173.2º, 18.6º and -172.8º, respectively. This is the consequence of the combined effect of asymmetry interaction of amino group and the hydrogen bridge existing between the oxygen atom (O_8) with the hydrogen atom (H_{13}) of hydroxyl group which contributes to decrease the conjugation interaction between the amide group and the benzene moiety (Mehmet Karabacak *et al.,* 2009). The calculated dihedral angles of C_1–C_2–C_3–C_4, C_2–C_3–C_4–C_5, C_3–C_4–C_5–C_6, C_4–C_5–C_6–C_1, C_5–C_6–C_1–C_2 and C_6–C_1–C_2–C_3 are as tabulated in table 4 and are deviated from 0º which confirm that the benzene ring is non-coplanar.

Table.1 Total energies of different conformations of 2HBA calculated at the DFT (B3LYP)/6-31G** level of theory

Conformer[+]	Total energies in Hartrees (6-31G*)	Energy Difference ΔE with respect to 'b' conformer in kJ/mol
a[**]	-476.200269070	0.00000000
b	-476.178953430	-55.56921050
c	-476.188784010	-29.75902080
d	-476.188899170	-29.45666820

[+] Forlabeling of conformers refer Fig.1
[**]Global minimum energy.

Table.2 Optimized bond lengths of 2HBA as monomer and dimer in comparison with XRD data

Bond lengths	Dimer (Å)	A (Å)	B (Å)	D (Å)	XRD data (Å)	Mean deviation from XRD in monomer (Å)	Mean deviation from XRD in dimer (Å)
C_1-C_2	1.422	1.422	1.418	1.409	1.401	-0.021	-0.025
C_2-C_3	1.407	1.407	1.404	1.399	1.401	-0.006	-0.01
C_3-C_4	1.385	1.386	1.388	1.392	1.401	0.015	0.012
C_4-C_5	1.403	1.403	1.395	1.396	1.401	-0.002	0.006
C_5-C_6	1.386	1.386	1.39	1.39	1.401	0.015	0.011
C_6-C_1	1.409	1.408	1.406	1.402	1.401	-0.007	-0.012
C_1-C_7	1.484	1.481	1.506	1.512	1.511	0.03	0.014
C_7=O_8	1.262	1.246	1.224	1.229	1.225	-0.021	-0.017
C_2-O_{12}	1.340	1.339	1.355	1.375	-	-	-
O_{12}-H_{13}	0.995	0.996	0.967	0.966	-	-	-
C_7-N_9	1.342	1.363	1.374	1.36	1.38	0.017	-0.002
N_9-H_{10}	1.025	1.01	1.007	1.008	1.022	0.012	-0.008
N_9-H_{11}	1.005	1.006	1.004	1.007	1.022	0.016	0.012
C_3-H_{14}	1.085	1.085	1.088	1.088	1.112	0.027	0.005
C_4-H_{15}	1.086	1.086	1.086	1.086	1.112	0.026	0.004
C_5-H_{16}	1.085	1.085	1.085	1.085	1.112	0.027	0.005
C_6-H_{17}	1.086	1.086	1.085	1.085	1.112	0.026	0.004

Table.3 Optimized valence angles of 2HBA as monomer and dimer in comparison with XRD data

Bond angles	Dimer(°)	A(°)	B(°)	D(°)	XRD data(°)	Mean deviation from XRD in (°) monomer	Mean deviation from XRD in dimer(°)
C_2-C_1-C_6	118.3	118.6	117.2	117.7	118.1	-0.5	-0.2
C_2-C_1-C_7	118.7	118.1	120.9	126.7	119.3	1.2	0.6
C_6-C_1-C_7	123.0	123.3	122.0	115.6	122.5	-0.8	-0.5
C_1-C_7=O_8	120.1	121.8	123.3	120.5	119.7	-2.1	-0.4
C_3-C_2-C_1	119.6	119.4	119.9	120.6	120.5	1.1	0.9
C_1-C_2-O_{12}	122.8	122.6	120.2	119.5	121.7	-0.9	-1.1
C_3-C_2-O_{12}	117.6	118.0	120.0	120.0	117.8	-0.2	0.2
C_2-O_{12}-H_{13}	105.8	106.1	108.3	109.3			
C_1-C_7-N_9	120.1	118.8	116.8	117.8	119.1	0.3	-1
C_7-N_9-H_{10}	119.2	115.7	115.7	116.7			
C_7-N_9-H_{11}	119.2	121.6	125.5	122.2			
H_{10}-N_9-H_{12}	119.0	117.7	118.8	121.2	118.8	1.07836	-0.21529
N_9-C_7-O_8	119.8	119.4	120	121.7			
C_2-C_3-C_4	120.5	120.4	121.3	120.4	120.2	-0.2	-0.3
C_4-C_3-H_{14}	121.7	121.7	120	120.3			
C_2-C_3-H_{14}	117.7	117.9	118.7	119.3			
C_3-C_4-C_5	120.6	120.8	119.7	120	119.7	-1.1	-0.9
C_3-C_4-H_{15}	119.5	119.4	119.7	119.5			
C_5-C_4-H_{15}	119.9	119.8	120.6	120.6			
C_4-C_5-C_6	119.2	119.2	119	119.3	120.8	1.6	1.6
C_4-C_5-H_{16}	120.6	120.5	120.8	120.3			
C_6-C_5-H_{16}	120.2	120.3	120.2	116.3			
C_5-C_6-C_1	121.8	121.6	123	122.1	120.7	-0.9	-1.1
C_5-C_6-H_{17}	118.1	118.6	120	116.3			
C_1-C_6-H_{17}	120.1	119.8	117.3	121.5			

Fig1. Various conformers of 2HBA

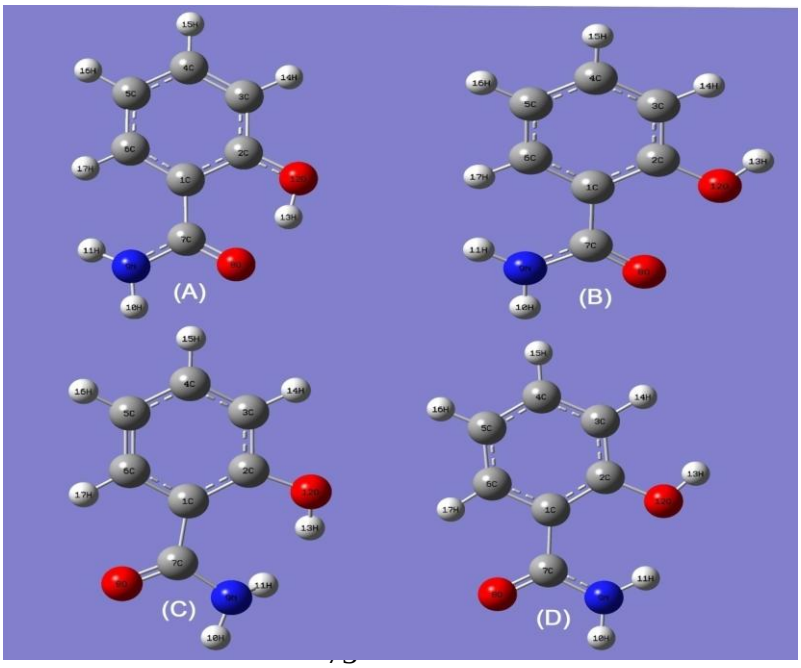

Table.4 Optimized dihedral angles of 2HBA as monomer

Dihedral angles	(º)
C_1-C_2-C_3-C_4	1.154
C_2-C_3-C_4-C_5	0.169
C_3-C_4-C_5-C_6	-0.724
C_4-C_5-C_6-C_1	-0.062
C_5-C_6-C_1-C_2	1.363
C_6-C_1-C_2-C_3	-1.89
C_7-C_1-C_2-C_3	178
C_7-C_1-C_6-C_5	-178.5
O_8-C_7-C_1-C_2	7.317
O_8-C_7-C_1-C_6	-172.8
N_9-C_7-C_1-C_2	-173.5
N_9-C_7-C_1-C_6	6.327
H_{10}-N_9-C_7-C_1	173.2
H_{11}-N_9-C_7-C_1	18.6
O_{12}-C_2-C_3-C_4	-179
O_{12}-C_2-C_1-C_6	178.2
H_{13}-O_{12}-C_2-C_3	177.5
H_{13}-O_{12}-C_2-C_1	-2.594
H_{14}-C_3-C_4-C_5	-179.3
H_{15}-C_4-C_5-C_6	179.8
H_{16}-C_5-C_6-C_1	-179.6
H_{17}-C_6-C_1-C_2	-176.9
H_{17}-C_6-C_5-C_4	178.2

Fig.2 Potential energy map of conformers of 2HBA

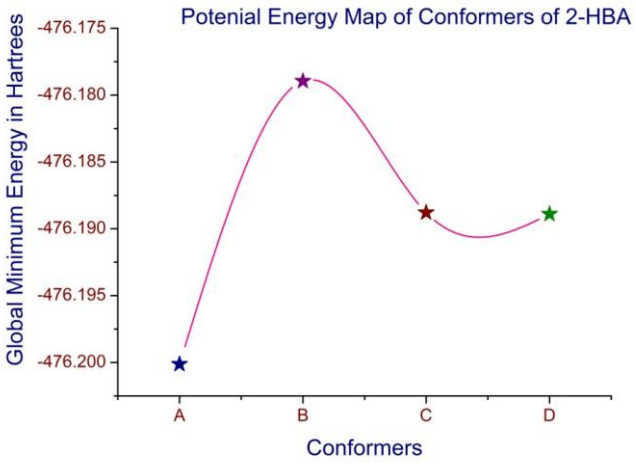

Table.5 Selected second-order perturbation energies E(2) (donor, acceptor) from natural bond orbital analysis

Conformer	Donor (i)	Type	ED/e	Acceptor (j)	Type	ED/e	E(2)[a] (kcal mol^{-1})	E(j)−E(i)[b] (a.u.)	F(i, j)[c] (a.u.)
Monomer									
A	O_8	LP (1)	1.96364	O_{12}- H_{13}	σ*	0.07276	6.63	1.11	0.077
	O_8	LP (2)	1.84760	O_{12}- H_{13}	σ*	0.07276	26.6	0.75	0.128
B					-				
D	O_{12}	LP (1)	1.97698	N_9- H_{11}	σ*	0.02440	7.34	1.11	0.081
Dimer									
A	O_8	LP (1)	1.93966	O_{12}- H_{13}	σ*	0.07192	9.91	1.14	0.095
	O_8	LP (2)	1.85259	O_{12}- H_{13}	σ*	0.07192	23.77	0.74	0.120
From unit 1 to unit 2									
A	O_8	LP (1)	1.93966	N_{26}- H_{27}	σ*	0.04752	10.75	1.18	0.101
	O_8	LP (2)	1.85259	N_{26}- H_{27}	σ*	0.04752	5.49	0.77	0.06
From unit 2 to unit 1									
A	O_{25}	LP (1)	1.93966	N_9- H_{10}	σ*	0.04752	10.75	1.18	0.101
	O_{25}	LP (2)	1.85259	N_9- H_{10}	σ*	0.04752	5.49	0.77	0.06

Table.6 Details of occupancy for selected NBOs

NBO	Occupancy			
	Dimer	A	B	D
O_8 LP (1)	1.93966	1.96364	1.97758	1.97698
O_8 LP (2)	1.85259	1.84760	1.86174	1.86141
O_{12}- H_{13} (σ*)	0.07192	0.07276	0.01101	0.00949
N_9- H_{10} (σ*)	0.04752	0.0114	0.00923	0.01129
N_9- H_{11} (σ*)	0.01158	0.00948	0.01423	0.0244
C_7- O_8 (σ*)	0.0145	0.02067	0.00976	0.01003

Table.7 Changes of electron density for selected NBOs

NBO	Changes of electron density
O_8 LP (1)	-0.02398
O_8 LP (2)	0.00499
N_9- H_{10} (σ*)	0.03612
N_9- H_{11} (σ*)	0.0021
C_1- C_7 (σ*)	-0.00442

Fig.3 Molecular structure of dimer of 2HBA

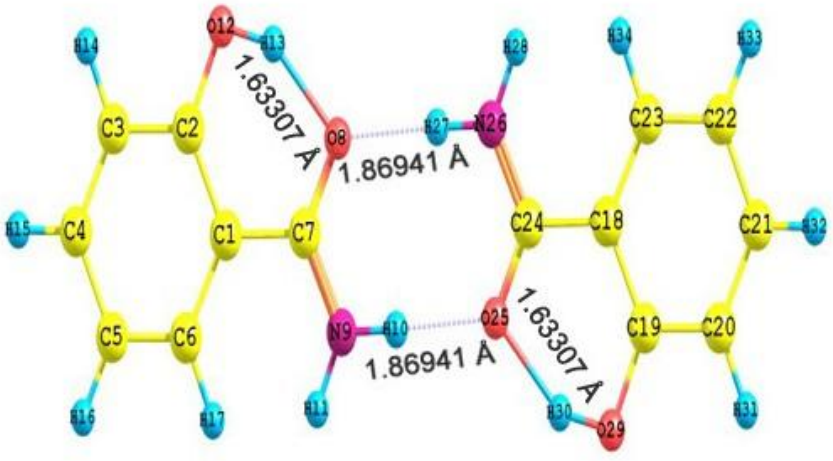

Conformer A as dimer with hydrogen bonded distance

Table.8 Definition of internal coordinates of 2HBA

No(i)	Symbol	Type	Definition
Stretching			
1-4	r_i	C-H	C3-H13,C4-H14,C5-H15,C6-H16
5-10	r_i	C-C(Ring)	C1-C2,C2-C3,C3-C4,C4-C5,C5-C6,C6-C1
11	r_i	C-C_a	C1-C7
12	r_i	C=O	C7-O8
13	r_i	C-N	C7-N9
14	r_i	C-O	C2-O12
15	r_i	O-H	O12-H13
16-17	r_i	N-H	N9-H10,N9-H11
In-plane bending			
18-19	β_i	C-C	C7-C1-C2,C7-C1-C6
20-27	β_i	C-H	C2-C3-H14,C3-C4-H14,C3-C4-H15,C4-C5-H15, C4-C5-H16,C5-C6-H16, C5-C6-H17.C1-C-6H17.
28	β_i	C=O	O11-C7-C1
29	β_i	C-N	N9-C7-C1
30-31	β_i	N-H-C	H10-N8-C7, H11-N8-C7
32	β_i	H-N-H	H10-N8-H11
33-34	β_i	C-O	O12-C2-C3, O12-C2-C1
35	β_i	O-H	H13-O12-C2.
36-41	β_i	C-C-C(Ring)	C1-C2-C3,C2-C3-C4,C3-C4-C5, C4-C5-C6,C5-C6-C1,C6-C1-C2
Out-of-plane bending			
42	ω_i	C-C	C7-C1-C2-C6
43	ω_i	C-O	O12-C2-C3-C1
44	ω_i	C=O	C1-C7-O11-N8
45-48	ω_i	C-H	H17-C6-C1-C5, H16-C5-C4-C6, H15-C4-C5-C3, H14-C3-C4-C2.
49	ω_i	N-H	C7-N8-H9-H10
Torsion			
50-55	τ_i	ring	C1-C2-C3-C4,C2-C3-C4-C5,C3-C4-C5-C6, C4-C5-C6-C1,C5-C6-C1-C2, C6-C1-C2-C3
56-59	τ_i	NO	O8-C7-C1-C2, O8-C7-C1-C6, N10-C7-C1-C2, N10-C7-C1-C6
60, 61	τ_i	O-H	H13-O12-C2-C3. H13-O12-C2-C1.
62-65	τ_i	NH	H10-N9-C7-C1, H10-N9-C7-O8, H11-N9-C7-C1, H11-N9-C7-O8.

For numbering of atoms refer Fig. 1

Table.9 Definition of local symmetry Coordinates of 2HBA

No(i)	Symbol[a]	Definition[b]
1-4	CH	r_1,r_2,r_3,r_4
5-10	CC	$r_5,r_6,r_7,r_8,r_9,r_{10}$
11	C-C_a	r_{11}
12	C=O	r_{12}
13	CN	r_{13}
14	CO	r_{14}
15	OH	r_{15}
16	NH_2ss	$(r_{16}+r_{17})/\sqrt{2}$
17	NH_2 as	$(r_{16}-r_{17})/\sqrt{2}$
18	bCC	$(\beta_{18}-\beta_{19})/\sqrt{2}$
19-22	bCH	$(\beta_{20}-\beta_{21})/\sqrt{2}$, $(\beta_{22}-\beta_{23})/\sqrt{2}$, $(\beta_{24}-\beta_{25})/\sqrt{2}$, $(\beta_{26}-\beta_{27})/\sqrt{2}$
23	bC=O	β_{28}
24	bC-N	β_{29}
25	NH_2 sc	$(2\beta_{30}-\beta_{31}-\beta_{32})/\sqrt{6}$
26	NH_2 rock	$(\beta_{30}-\beta_{31})/\sqrt{2}$
27	bCO	$(\beta_{33}-\beta_{34})/\sqrt{2}$
28	bOH	β_{35}
29	bring	$(\beta_{37}-\beta_{36}+\beta_{39}-\beta_{38}+\beta_{41}-\beta_{40})/\sqrt{6}$
30	bring	$(2\beta_{36}-\beta_{37}+2\beta_{39}-\beta_{40}-2\beta_{41})/\sqrt{12}$
31	bring	$(\beta_{37}-\beta_{38}+\beta_{40}-\beta_{41})/2$
32	ωCC_a	ω_{42}
33	ωCO	ω_{43}
34	ωNO	ω_{44}
35-38	ωCH	$\omega_{45},\omega_{46},\omega_{47},\omega_{48}$
39	ωNH_2	ω_{49}
40	τring	$(\tau_{51}-\tau_{50}+\tau_{53}-\tau_{52}+\tau_{56}-\tau_{55})/\sqrt{6}$
41	τring	$(\tau_{50}-\tau_{52}+\tau_{53}-\tau_{55})/2$
42	τ ring	$(\tau_{50}+2\tau_{51}-\tau_{52}-\tau_{53}+2\tau_{54}-\tau_{55})/\sqrt{12}$
43	τ NO	$(\tau_{56}+\tau_{57}+\tau_{58}+\tau_{59})/4$
44	τ OH	$(\tau_{60}+\tau_{61})/2$
45	τNH_2	$(\tau_{62}+\tau_{63}+\tau_{64}+\tau_{65})/4$

[a]These symbols are used for description of normal modes by TED in Table.10
[b]The internal coordinates used here are defined in Table.8

Table.10 Observed and B3LYP/6-31G** level calculated vibrational frequencies (in cm^{-1}) of 2HBA

No	Observed frequency(cm^{-1})		Calculated frequency (cm^{-1}) with B3LYP/ 6-31G**force field				TED (%) among type of internal coordinates [c]
	IR	Raman	Unscaled	Scaled	IR[a](A_i)	Raman[b](I_i)	
1	3397vs	-	3743	3397	42.88	56.14	υNH_{2asym}(99)
2	3191vs	-	3609	3191	50.72	130.4	υNH_{2sym}(99)
3	3096ms	-	3246	3096	439.9	81.40	υOH(99)
4	3061ms	3063w	3218	3061	2.910	117.2	υCH(98)
5	2966m	-	3210	2968	20.83	183.5	υCH(98)
6	2954m	-	3188	2952	11.165	84.258	υCH(99)
7	2924m	-	3178	2924	10.635	48.529	υCH(99)
8	1674vs	-	1732	1689	201.602	11.757	υC=O(26), υCC(11),$bNH_{2\ sci}$(11), bCC_a(10)
9	1666vs	-	1668	1664	201.696	19.213	υCC(38), $bNH_{2\ sci}$(19), bCH(18), υCN(11)
10	1622vs	1627w	1640	1625	55.940	19.744	υCC(45), bCH(25), bOH(11)
11	1596vs	-	1539	1592	53.205	6.807	$bNH_{2\ sci}$(30), bCH(17), υCC(15), bOH(10)
12	1591sh	-	1499	1574	129.641	2.206	υCC (48), bCH (21)
13	1505s	-	1454	1519	25.676	4.440	υCC (55), bOH(13),
14	1448vs	1451w	1417	1451	222.309	61.733	υCN(25), υCCa (17), bNH_{2rock}(13), bC=O(13)
15	1426s	-	1365	1415	107.271	1.624	bOH(21), υCC(20), bCH(20), υCN(13)
16	1359vs	-	1417	1359	62.069	23.000	bCH (41), υCC (22), υCO(17)
17	1307m	1307w	1365	1307	28.706	2.538	υCO(41), υCC(21), bCH(17)
18	1253vs	-	1313	1275	101.289	10.804	υCC(47), bCH(24), bOH(11)
19	-	1249vs	1268	1228	42.968	8.101	υCC(64), bCH(31)
20	1169m	-	1166	1172	5.184	9.232	bCH (47), υCC (22),
21	1120m	1128w	1120	1122	21.130	17.533	$bNH_{2\ rock}$ (24), υCC(24), υCCa(15), υC=O(13),
22	1083m	1087w	1087	1070	14.574	16.811	bCH(23), $bNH_{2\ rock}$(20), υCN(18), bring(15), υC=O(13)
23	1021w	-	1060	1025	11.640	15.915	bCH (72)
24	878m	-	988	885	0.320	0.546	ωCH(88)

25	849m	-	935	855	4.841	5.021	bring(65), υCC(12)
26	855sh	851w	871	848	0.726	0.398	ωCH(81)
27	785m	-	863	809	1.223	3.101	ωCH(30), tring(27), gCO(18), ωCC_a(14)
28	780sh	-	859	776	47.071	1.083	τOH(36), ωNO(18), ωCH(15), ωCCa(12), τ ring (12)
29	759 vs	-	783	757	60.459	2.609	τ ring(47), ωCH(36)
30	751vs	750sh	758	746	4.449	22.129	υCC_a(34), bring(28),υCC(10)
31	721w	-	741	720	4.180	0.757	ωCH(47), ωCO(22),τ ring(15)
32	704	-	704	696	66.581	1.724	τ ring(72), ωCH(11)
33	661s	-	645	661	40.831	1.028	bC=O(42), bring(33)
34	611sh	-	570	608	5.301	8.791	bring(45), υCC(18), bCCa(12)
35	553w	556w	553	555	29.392	3.505	ωNH_2(58),τ ring (19), ωCC_a(9)
36	530m	522w	537	537	2.397	1.476	bCN(18), ωCO(17), τ ring(13), bCO(10)
37	517m	517m	506	522	1.957	1.843	bCO(34), τ ring (19), ωCH(10), bCN(7), bCO(6)
38	-	455m	443	444	3.630	4.719	ωCO(35), bCO(21), bCN(13)
39	-	420w	420	421	16.836	1.278	τ ring(58), ωCC_a (23)
40	-	395w	379	387	10.869	0.958	bring(35), υCC_a(18), bCO(16)
41	-	332	331	337	134.893	3.948	bCC_a(63), bCN(19)
42	-	301m	257	287	75.418	0.837	ωNO(27), bCC_a(23), bCN(19)
43	-	249m	249	247	0.901	1.731	ωCC_a(40), τring(27), ωCH(10)
44	-	149s	142	143	0.548	2.663	τ NH_2(34), τ ring(23), ωCC_a(19), τring(12)
45	-	-	70	71	7.730	0.516	τNO(64), τOH(13)

Abbreviations used: R,ring; υ-stretching; b, bending; asym, asymmetric; sym, symmetric; sci, scissoring; rock, rocking; ω, wagging; τ, torsion; NH_2, amino; OH, hydroxyl;

[a]Relative absorption intensities normalized with highest peak absorption equal to 1.0.

[b]Relative Raman intensities calculated by Eq. 2 and normalized to 100

[c]For the notations used see Table. 8

Table.11 The dipole moment (μ) and first-order hyperpolarizibility (β) of2HBAderived from DFT calculations

β_{xxx}	-2.1027
β_{xxy}	-48.61
β_{xyy}	1.0303
β_{yyy}	-82.332
β_{zxx}	849.36
β_{xyz}	390.95
β_{zyy}	421.8
β_{xzz}	-4120.9
β_{yzz}	-550.58
β_{zzz}	166.5
β_{total}	1.744
μ_x	0.00018571
μ_y	2.42117708
μ_z	0.09221304
μ	1.58542607

Dipole moment (μ) in Debye, hyperpolarizibilityβ(-2ω;ω,ω) 10^{-30}esu.

Fig.4 FT-IR spectra of 2HBA (a) Calculated (b)and (c) Observed with B3LYP/6-31G**

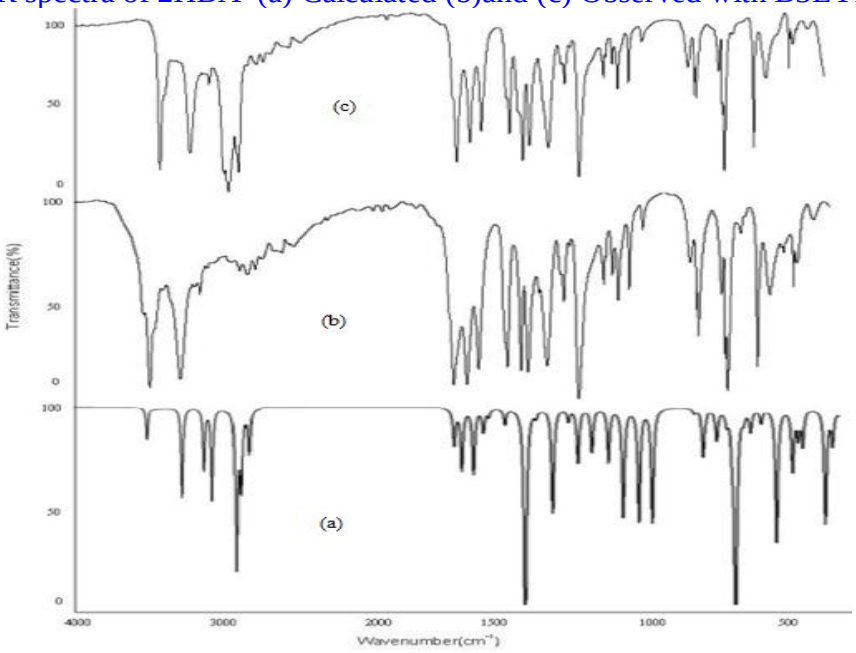

Fig.5 FT-Raman spectra of 2HBA (a) Calculated (b) Observed with B3LYP/6-31G**

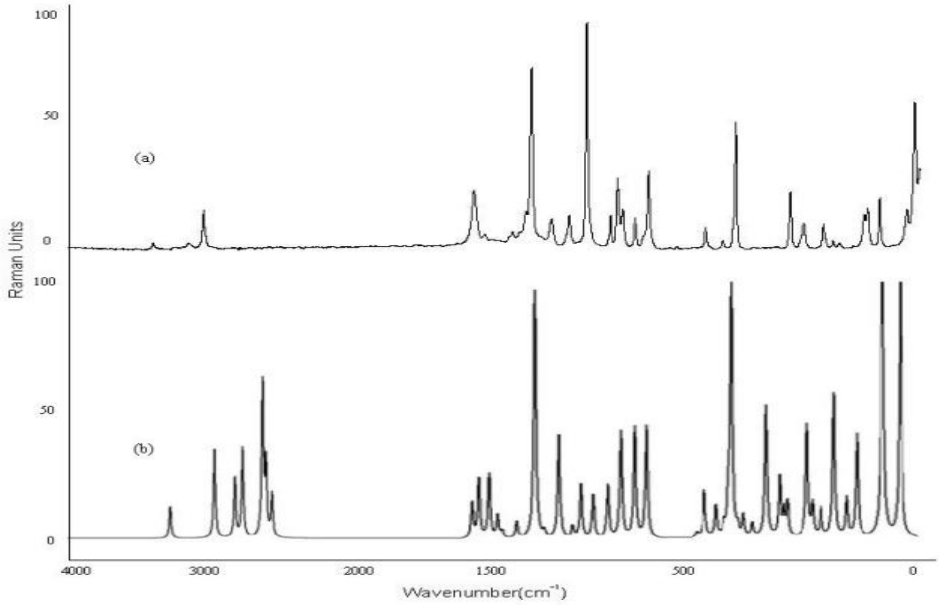

Fig.6 Molecular electrostatic potential maps of conformers and dimer of 2HBA

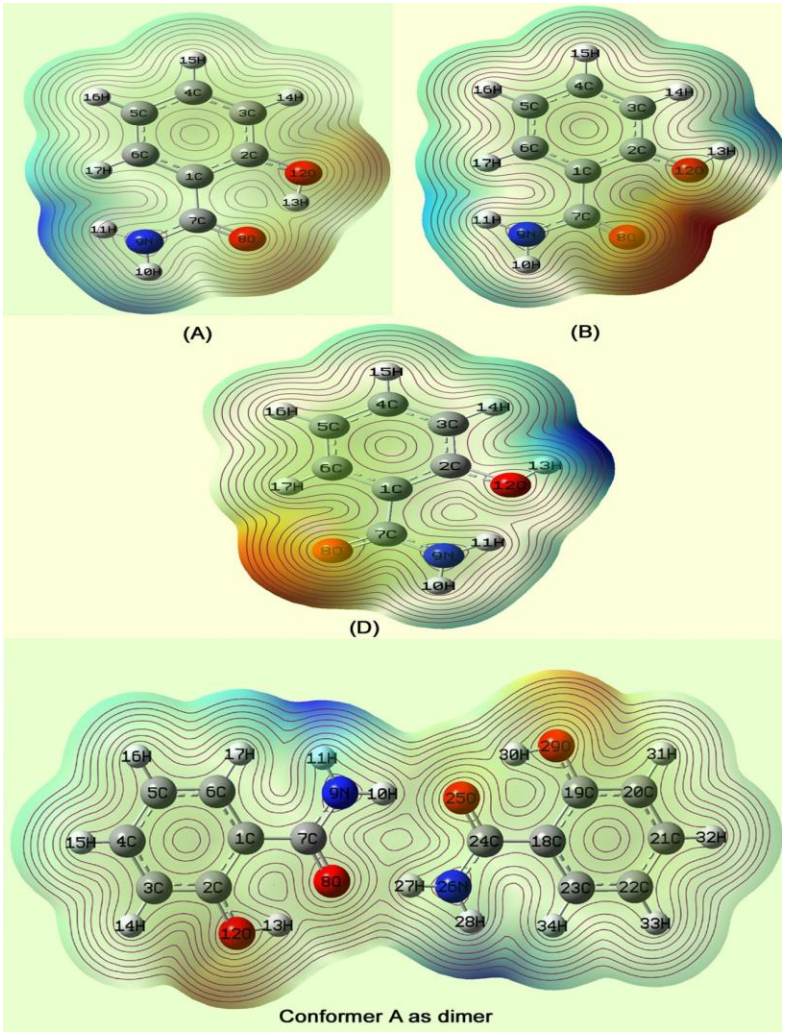

Fig.7 Representation of the orbital involved in the electronic transition for (a) HOMO (b) LUMO (c) HOMO, LUMO (d) Occupied (e) Virtual (f) All

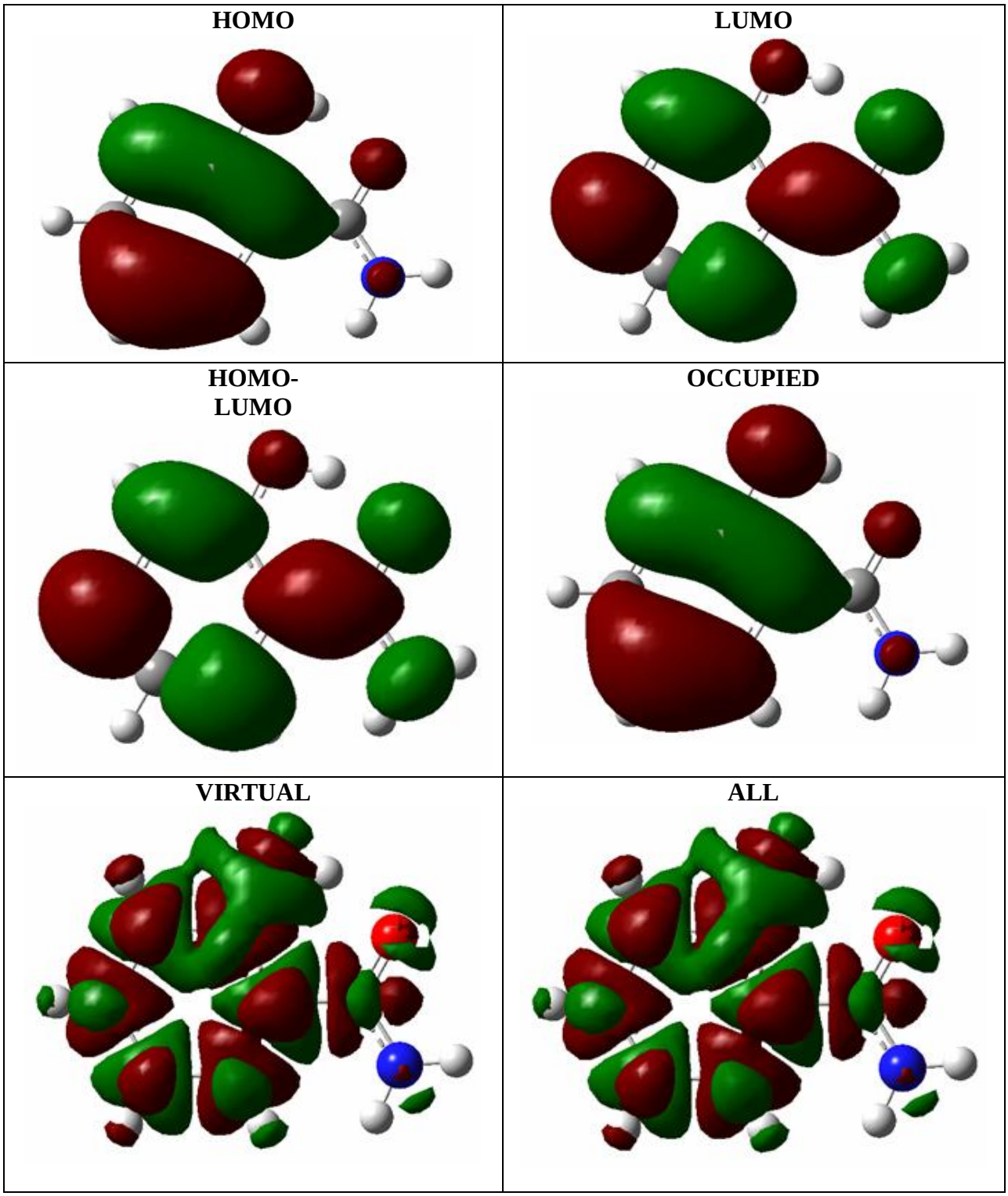

Generally all the bond angles show slight deviations from 120º of sp^2 hybridization in benzene ring due to inductive effect caused by hydroxyl group and amide group. With the electron donating and withdrawing substituents on the benzene ring, the symmetry of the ring is distorted, yielding ring angles smaller than 120º at the point of amide group substitution and hydroxyl group substitution. As the amide and hydroxyl moieties involve in the hydrogen bonding, the impact of inductive effect has been reduced. This is noticeable by comparing the bond angles in all conformers. The interaction of amino group of amide with the substituent on the ring is of great importance in determining its structural properties. Amino group and its derivatives are known to have pyramidal geometry resulting from a balance between opposing forces, the stability gained by the molecule as a whole arising from p–π conjugation of the nitrogen lone pair with the aromatic system versus that gained by the nitrogen using highly directed sp^3 orbital for bond formation (Palafox and Melendez, 1999).

The decrease of endocyclic angle at C_6-C_1-C_2 (118.6º) and increase of exocyclic angle at C_6-C_1-C_7(123.3º) ratify the above statements, whereas exocyclic angle at C_3-C_2-O_{12} displays a decrease (118º), due to hydroxyl substitution (Arjunan *et al.*, 2011). The decrease of exocyclic angle can be explained in terms of hybridization effects which makes the carbon atom carrying the substituent is pushed inside the ring towards the ring centre, due to hydroxyl substitution. Highly electronegative oxygen in hydroxyl group tends to attract more of the p character in the hybrid orbital towards itself thereby increasing the s character in the other two hybrid orbitals, which accounts for the shortening of the C-C bonds and increase of the angle between them (Doraisamy, S.D. Sharma, 1983). The decrease of deformation angle H_{13}-O_{12}-C_2 is due to hydrogen bonding which was explained in detail in the section 3.2.

From the structural data, it is observed that the various C–C bond distances calculated between the ring carbon atoms and the C–H bond length are found to be consistent with the literature. The influence of the substituent on the molecular parameters is spectacular in the bond lengths of benzene ring. The substitution of amide group and hydroxyl group atom holds the responsibility of elongation and contraction of C-C bonds.

Vibrational properties

Normal coordinate analysis was performed to provide a complete assignment of the fundamental vibrational wave numbers of the molecules. For this purpose, the full set of 63 standard internal coordinates (containing 18 redundancies) for 2HBA were defined as given in Table 8. From these, a non-redundant set of 45 local symmetry coordinates were constructed by suitable linear combinations of internal coordinates following the recommendations of Fogarasi and Pulay, (1985) (Fogarasi *et al.*, 1992). These coordinates are summarized in Table 9. The theoretically calculated DFT force fields were transformed to this latter set of symmetry coordinates and used in all subsequent calculations. The total energy distribution (TED) for each normal mode among the symmetry coordinates of the molecules was calculated. A complete assignment of the fundamentals was proposed based on the calculated TED values, Infrared band intensities and Raman activities. The unscaled B3LYP/6-31G** vibrational frequencies are generally larger than the experimental value. This is partly due to the

neglect of anharmonicity and partly due to approximate nature of the quantum mechanical methods.

However for reliable information on the vibrational properties, the use of selective scaling is necessary. The calculated wavenumbers are scaled using the set of transferable scale factors recommended by Rauhut and Pulay (1995).

The experimental assignments of FT-IR and FT-Raman for several vibrational frequencies of 2HBA are shown in table 10. The theoretically predicted wave numbers for the various fundamental vibrational modes by density functional methods using 6-31G** basis set have been collected in Table 10. The title molecule belonging to C_S point group has 45 normal modes of fundamental vibrations. The main focus of the present investigation is the proper assignment of the experimental frequencies to the various vibrational modes of 2HBA in collaboration with the scaled down calculated harmonic vibrational frequencies at B3LYP level using6-31G** basis set.

Comparison of the frequencies calculated at B3LYP level with the experimental values reveals the overestimation of the calculated vibrational modes due to neglect of anharmonicity in real system. Inclusion of electron correlation in density functional theory to a certain extent (lowers the frequency values) makes the frequency values smaller. Reduction in the computed harmonic vibrations, though basis set sensitive is only marginal as observed in the DFT values using 6-31G** basis set. In the last column a detailed description of the normal modes based on the potential energy distribution (PED) is given. On the basis of our calculations and recorded experimental data, we made a reliable one to one correspondence between observed fundamentals and any of the frequencies calculated by the B3LYP method. The assignments are based on the PED and the vibrational animations of fundamentals using the GAUSSVIEW package program in the B3LYP/6-31G**calculations.

For visual comparison, the observed and simulated FT-IR and FT-Raman spectra were presented in Figs. 4 and 5 respectively. Root mean square (RMS) values of wave numbers were obtained using the following expression:

$$RMS = \sqrt{\frac{1}{n-1}\sum_i^n \left(\upsilon_i^{calcu} - \upsilon_i^{exp}\right)^2} \quad \text{.....(4)}$$

The RMS error of wave numbers (unscaled /B3LYP/6-31G**) obtained for 2HBA was found to be 138cm^{-1}. In order to reproduce the observed wave numbers, refinement of scaling factors was applied and optimized via least square refinement algorithm which resulted in a RMS deviation of 9.11 cm^{-1}.

C–H vibrations

Aromatic compounds commonly exhibit multiple bands in the region 3100–3000 cm^{-1} due to aromatic C–H stretching vibrations. The 2HBA has four adjacent C–H moieties in benzene ring. In the present work of 2HBA, the medium to strong bands identified at 3061, 2966, 2954 and 2924 cm^{-1} in FT-IR spectrum are assented as C-H stretching modes (George Socrates, 2001). The computationally predicted wavenumbers of the C-H stretching vibrations show very good agreement with experimental data. The TED of these C-H stretching vibrations is pure and it is almost contributing to 100%. In the Infrared spectra of aromatic compounds, the C-H in plane deformation modes normally occurs in the region of 1200-900 cm^{-1} (Sathyanarayana, 1996). In this region a number of

interactions are possible, thus necessitating great care in the interpretation of bands. Additional difficulties are also there due to the presence of C-C stretching and hydroxyl group vibrations accomplished with amino group deformation vibrations. The bands due to C–H in plane ring bending vibration interacting somewhat with C–C stretching vibration are observed as a number of m-w intensity sharp bands in the region 1500–1025 cm^{-1}. The in plane bending modes are attributed to the FTIR bands present at 1359, 1169, 1083 and 1021 cm^{-1} in2HBA (Arjunan *et al.,* 2011; George Socrates, 2001; Sathyanarayana, 1996). C–H out-of-plane bending vibrations are strongly coupled vibrations and occur in the region 848–692 cm^{-1} (George Socrates, 2001). The wagging vibrations are characterized by the FT-IR bands present at 878, 855, 785 and 721 cm^{-1} in 2HBA (Arjunan *et al.,* 2011; Sheena Mary *et al.,* 2011; Yu Zhang *et al.,* 2013). Both the in-plane and out-of-plane bending vibrations are described as mixed modes. The above conclusions are in very good agreement with literature values.

Ring vibrations

The ring stretching vibrations are very much important in the spectrum of benzene and its derivatives and are highly characteristic of the aromatic ring itself. The ring carbon–carbon stretching vibrations occur in the region 1430–1625 cm^{-1}. For aromatic six membered rings there are two to three bands in this region due to skeletal vibrations (George Socrates, 2001; Sathyanarayana, 1996). In the present work, the observed and calculated wave numbers are in excellent agreement with the literature. The FT-IR bands identified at 1666, 1622, 1591, 1505, 1253 and 1249 cm^{-1} and FT-Raman band at 1619 cm^{-1} in 2HBA are attributed to C=C stretching vibrations (Arjunan *et al.*, 2011). The peaks identified at 1666 and 1622 are due to the quadrant stretching vibrations (Jag Mohan, 2001). The bands at about 1591 cm^{-1} and 1359 cm^{-1} are due to semicircle stretching vibrations (Jag Mohan, 2001). The intensity of the band at 1532 cm^{-1} is weak band for ring conjugated with carbonyl groups (George Socrates, 2001; Yu Zhang *et al.,* 2013). It is well proven in the present study. The ring deformation vibrations are ascribed to the FT-Raman bands at 849, 611 and 395 cm^{-1} in 2HBA (George Socrates, 2001; Sheena Mary *et al.,* 2011). The out of plane deformations are established at 757,696 and 431 cm^{-1} in FT-IR spectra of 2HBA (Sathyanarayana, 1996; Sheena Mary *et al.,* 2011). The calculated C–C out-of-plane and in-plane bending modes have been found to be consistent with the recorded spectral values.

O-H group vibrations

Special attention is required for O-H vibrations of the title molecule. It has been demonstrated in section 4.2.1 that, while the band arising from the stretching vibration of the free hydroxyl group appears in the range of 3690–3600 cm^{-1}, the vibration of the hydrogen bonded hydroxyl group in 2HBA gives rise to a band at 3096 cm^{-1}. In 2HBA, the band arising from the stretching vibrations of the bonded hydroxyl group cannot be straightforwardly identified in the experimental spectrum because the band is located in the region of the υ(C-H) vibrations. This overlapping of bands is due to the intermolecular hydrogen bonding enduring between carbonyl and hydroxyl group. The molecular structure of title compound also circumstantiates the above assignment supported by the literature (George Socrates, 2001; Sathyanarayana, 1996; Yaping Tao *et al.,* 2015). The O-H stretching modes are weakly polarized therefore they are generally not observed in the Raman spectrum. For instance, as in the

case observed for O-H vibrations, O-H groups, which possess intra and inter molecular hydrogen bonding, have lower line width in FT-Raman spectrum. The in plane deformation vibrations of hydroxyl group occur at 1365 cm^{-1} in 2HBA of IR spectra and are in agreement with the literature (George Socrates, 2001; Sathyanarayana, 1996). The C-O stretching vibrations are observed at 1307 cm^{-1} in 2HBA with of IR band [142]. The out of plane bending modes are found at 780 cm^{-1} in 2HBA of Raman spectrum and the assignments are believed to be unambiguous (George Socrates, 2001; Sebastian *et al.*, 2013; Rajeev *et al.*, 2014). The theoretically scaled values also show exact correlation with our measured experimental data as well as literature data.

Amide group vibrations

The molecule under consideration possesses amide group in ring and hence eleven internal modes of vibrations are possible such as: (i) NH_2 symmetric stretching, (ii) NH_2 asymmetric stretching, (iii) NH_2 scissoring, (iv) NH_2 rocking, (v) NH_2 wagging, (vi) NH_2 torsion, (vii) C-N stretching, (viii) C-N in plane deformation, (ix) C=O stretching, (ix) C=O in plane deformation, (x) NO wagging and (xi) NO torsional mode.

The NH_2 group has two N-H stretching vibrations, one being asymmetric and the other symmetric. The frequency of asymmetric vibration is higher than that of symmetric one. In 2HBA, the very strong bands observed at 3397 and 3191cm^{-1} in the FT-IR are as-signed to asymmetric and symmetric stretching vibrations respectively. In the FT-Raman the weak bands at 3397and 3191cm^{-1} are assigned to NH_2 asymmetric and symmetric stretching mode. Based on the above conclusion, the theoretically scaled down wave numbers 3397 and 3191 cm^{-1} by B3LYP/6-31G** method are assigned to amino asymmetric and symmetric stretching vibrations respectively and show good agreement with the literature (Arjunan *et al.,* 2011; George Socrates, 2001). The PED confirms that these modes of vibration are pure as they do not mix with any other mode. The shifting of stretching modes of amino group to lower wave number region strongly indicates the presence of inter molecular hydrogen bonding (George Socrates, 2001). The (Amide II band) NH_2deformation vibration observed in FT-IR spectra has a very strong band at 1596 cm^{-1} is assigned to NH_2scissoring vibration. The theoretically scaled down values at 1592 cm^{-1} by B3LYP/6-31G** method is assigned to NH_2scissoring vibration lie well within the region of 1650–1590 cm^{-1} reported as in literature. The scaled down wave number by B3LYP/6-31G** at 1122cm^{-1} is assigned to NH_2 rocking vibration and from recorded spectra that the medium and a medium band observed in FT-IR and a weak band in FT-Raman spectra at 1128 cm^{-1} have to be assigned to this vibration. The frequency in the FT-IR spectrum at 553cm^{-1} assigned to NH_2wagging mode correlates with the frequency 555 cm^{-1} computed by the B3LYP/6-31G**method respectively. The NH_2twisting vibration (Amide VII band) computed by B3LYP/6-31G**method at 143cm^{-1} shows good agreement with the recorded FT-Raman frequency of 149cm^{-1}. The vibrational assignment of the fundamental modes is also supported by Gauss-view molecular visualization program. All the above assignments are in satisfactory agreement with the literature (Arjunan *et al.,* 2011; Sathyanarayana, 1996).

Generally the carbonyl group stretching vibration becomes the finger print of its

substituted compounds. In the present circumstance, it was greatly affected and made its appearance at 1674 cm^{-1} in FT-IR spectra. The FT-Raman counterpart is missing for this mode. Stretching vibration of C=O group (Amide I band) is expected to appear at 1715–1680 cm^{-1} (Yu Zhang *et al.*, 2013). The very strong C=O experimental bands in FT-IR spectra observed at 1674cm^{-1} for 2HBA corresponds to the stretching vibration of C=O group of amide lie in a lower frequency region, which is attributed to the conjugation effect and formation of hydrogen bonds (Balachandran *et al.*, 2014; Premkumar *et al.*, 2015). The increase in conjugation, generally, leads to intensification of infrared bands intensities. The conjugation and influence of intramolecular hydrogen bonding result in lowering of the stretching wave numbers of C=O vibration. Any deviation of the calculated wavenumber for this mode can be attributed to p-electron delocalization due to the conjugation or formation of hydrogen bonds. The calculated vibration for these bands are in excellent consistent with the experimentally obtained results. The identification of C-N vibrations (Amide III band) is very difficult task since mixing of several bands is possible in this region. However, with the help of theoretical calculations and percentage relative weight of vibrations the C-N stretching and deformation vibrations are identified and assigned in this study. Socrates *et al.* assigned vibrations in the region 1420–1400 cm^{-1} for amide III band which is C-N stretching (Doraisamy and Sharma, 1983). The C-N stretching modes are appeared at 1448 cm^{-1} for 2HBA in the solid-state FT-IR spectra. The FT-IR band observed at 1448$cm^{-1}$is the most intensive band in this region. This vibrational mode is found at 1451 cm^{-1} in FT-Raman spectra. The C-N in-plane bending vibration is observed as medium band at 530 cm^{-1} in FT-IR spectra and a weak band in FT-Raman. DFT (B3LYP/6-31G**) computed wave numbers of these bands show excellent agreement with corresponding experimental ones. Amide V and amide VI bands correspond to N-O wagging and N-O torsional vibrations. These modes are assigned unambiguously with the aid of literature (Arjunan *et al.*, 2011; George Socrates, 2001; Sathyanarayana, 1996).

Hyperpolarizability calculations

Frontier orbitals

The first-order hyperpolarizibility (β_{ijk}) of the novel molecular system of 2HBA is calculated using 6-31G** basis set based on finite field approach. Hyperpolarizibility is a third rank tensor that can be described by a 3 x 3 x 3 matrix. It strongly depends on the method and basis set used. The 27 components of 3D matrix can be reduced to 10 components due to Kleinman (1962) symmetry. The calculated first-order hyperpolarizability (β_{total}) of 2HBA is $1.744x10^{-30}$ esu, which is nearly 9 times greater than that of urea (0.1947×10^{-30}esu). The calculated dipole moment (μ) and first-order hyperpolarizibility (β) are shown in Table 11. The theoretical calculation seems to be more helpful in determination of particular components of β tensor than in establishing the real values of β. Domination of particular components indicates on a substantial delocalization of charges in those directions. It is noticed that in β_{zxx} (which is the principal dipole moment axis and it is parallel to the charge transfer axis) direction, the biggest values of hyperpolarizability are noticed and subsequently delocalization of electron cloud is more in that direction. The higher dipole moment values are associated, in general, with even larger projection of β_{total} quantities. The electric dipoles may enhance, oppose or at least bring the dipoles

out of the required net alignment necessary for NLO properties such as β_{total} values. The connection between the electric dipole moments of an organic molecule having donor–acceptor substituent and first hyperpolarizability is widely recognized in the literature (Prasad and Williams, 1991). The maximum β was due to the behavior of non-zero μ value. One of the conclusions obtained from this work is that non-zero μ value may enable the finding of a non-zero β value. Of course Hartee–Fock calculations depend on the mathematical method and basis set used for a polyatomic molecule.

Figure 7 shows the highest occupied molecule orbital (HOMO) and lowest unoccupied molecule orbital (LUMO) of 2HBA. There is an inverse relationship between hyperpolarizability and HOMO–LUMO.

HOMO energy = -0.315 a.u
LUMO energy = 0.086 a.u
HOMO–LUMO energy gap = 0.401 a.u

Conclusion

This study presents a facile and efficient conformational analysis of 2HBA. The computational analysis revealed some interesting features of these of compound in various possible conformations. The structural stability and hydrogen bonding was investigated at DFT/B3LYP/6-31G** level of theory for all conformers. The conformers were predicted to exist predominantly in the symmetric near-planar structure with C_s molecular symmetry with the possibility of hydrogen bonding. The global minimum energy is predicted to decrease when going from non hydrogen bonded to strongly hydrogen bonded derivatives. Hence it is concluded that hydrogen bridges are important driven forces in molecular structure optimization. The hydrogen atom of the amidemoiety and the oxygen atom of the amide moiety of another molecule are involved in a weak hydrogen bond forming a dimer, where the intermolecular $H_{27}...O_8$ distance is 1.86941 Å, but the intra molecular attraction is stronger than it and the distance $H_{13}...O_8$ is 1.63307 Å. NBO analysis and molecular electrostatic potential maps reveal the inter and intra molecular hydrogen bond in the structure corresponding to the conformer of global minimum energy. Theoretically predicted geometrical parameters substantiate that molecular circumstance favours the hydrogen bond and coincide with the XRD data. Molecular structure, vibrational frequencies, of 2HBA has been studied using DFT calculations. On the basis of the calculated and experimental results; assignment of the fundamental frequencies were examined. Good correlation is found between the computed and experimental wave numbers. The difference between the observed and scaled wave number values of most of the fundamentals is very small. Therefore, the assignments made at DFT level of theory with only reasonable deviations from the experimental values seem to be correct. Therefore, this study confirms that the theoretical calculation of vibrational frequencies for 2HBA is quite useful for the vibrational assignments and for predicting new vibrational frequencies. NBO result reflects the charge transfer within the molecule. The theoretically constructed FT-IR and FT-Raman spectra coincide with the experimentally observed spectra. HOMO, LUMO energies and HOMO-LUMO energy gaps has been also discussed.

References

Arjunan, V., Mythili, C.V., Mageswari, K., Mohan, S. 2011. *Spectrochim. Acta Part A*, 79: 249–253

Arjunan, V., Suja Ravi Isaac, A., Rani, T., Mythili, C.V., Mohan, S. 2011. *SpectrochimicaActa Part A.,* 78: 1625–1632

Balachandran, V., Santhi, G., Karpagam, V., Rastogi, V.K. 2014. *SpectrochimicaActa Part A: Mol. Biomol. Spect.,* 118: 835–846.

Becke, A.D. 1988. *Phys. Rev. A.,* 38: 3098–3100.

Becke, A.D. 1993. *J. Chem. Phys.,* 98: 5648–5652.

Cotton, F.A., Luck, R.L. 1989. *Inorg. Chem.,* 28: 3210–3213.

Doraisamy, S., Sharma, S.D. 1983. *J. Mol. Structure*, 102: 81–92.

Fogarasi, G., Pulay, P. 1985. In: J.R. Durig (Ed.), Vibrational spectra and structure, Vol. 14, Chap. 3. Elsevier, Amsterdam. 125 Pp.

Fogarasi, G., Zhou, X., Taylor, P.W., Pulay, P. *J. Am. Chem. Soc.,* 114: 8191–8201.

Foresman, J.B., Frisch, A. 1996. Exploring chemistry with electronic structure methods, second edn., Gaussian, Inc., Pittsburg, PA.

Forsyth, D.A., Sebag, A.B. 1997. *J. Am. Chem. Soc.*, 119: 9483–9494.

Frisch, M.J., Trucks, G.W., Schlegel, H.B., Scuseria, G.E., Robb, M.A., Cheeseman, J.R., Scalmani, G., Barone, V., Mennucci, B., Petersson, G.A., Nakatsuji, H., Caricato, M., Li, X., H.P. Hratchian, A.F. Izmaylov, J. Bloino, G. Zheng, J.L. Sonnenberg, M. Hada, M. Ehara, K. Toyota, R. Fukuda, J. Hasegawa, M. Ishida, T. Nakajima, Y. Honda, O. Kitao, H. Nakai, T. Vreven, J.A. Montgomery Jr., J.E. Peralta, F. Ogliaro, M.Bearpark, J.J. Heyd, E. Brothers, K.N. Kudin, V.N. Staroverov, R. Kobayashi, J. Normand,K. Raghavachari, A. Rendell, J.C. Burant, S.S. Iyengar, J. Tomasi, M. Cossi, N.Rega, J.M. Millam, M. Klene, J.E. Knox, J.B. Cross, V. Bakken, C. Adamo, J. Jaramillo,R. Gomperts, R.E. Stratmann, O. Yazyev, A.J. Austin, R. Cammi, C. Pomelli, J.W.Ochterski, R.L. Martin, K. Morokuma, V.G. Zakrzewski, G.A. Voth, P. Salvador,J.J. Dannenberg, S. Dapprich, A.D. Daniels, O. Farkas, J.B. Foresman, J.V. Ortiz, J.Cioslowski, D.J. 2009. Fox, Gaussian 09, Revision A.02, Gaussian, Inc., Wallingford, CT.

George Socrates, 2001. Infrared and Raman characteristic group frequencies–tables and charts, 3rd edn, John Wiley & Sons, Chichester.

Jag Mohan, Organic Spectroscopy, Principles and Applications, Second Edition, New Age International (p) Limited Publishers, New Delhi, (2001)

James, C., Amal, A., Raj, R., Reghunathan, I. Hubert Joe, V.S., Jayakumar, 2006. *J. Raman Spectrosc.,* 37: 1381–1392.

Karabacak Mehmet, Kurt Mustafa, 2009. *J. Mol. Struct.,* 919: 215–222.

Katritzky, A.R., Pozharski, A.F. 2000. Handbook of heterocyclic chemistry, second edn., Elsevier, Pergamon.

Kawski, P., Kochel, A., Perevozkina, M.G., Filarowski, A., *J. Mol. Struct.*, 790: 65–73.

Kleinman, D.A. 1962. *Phys. Rev.,* 126: 1977–1979

Lee, C., Yang, W., Parr, R.G. 1988. *Phys. Rev. B.,* 37: 785–789.

Mehmet Karabacak, Mustafa Kurt, Ahmet Atac, 2009. *J. Phys. Organic Chem.,* 22: 321–330.

Muniappan, P., Meenakshi, R., Rajavel, G., Arivazhagan, M. 2014. *Spectrochim. Acta Part A,* 117: 739–753.

Murray, J.S., Sen, K. 1996. Molecular electrostatic, potentials concepts and applications. Elsevier, Amsterdam.

Palafox, M.A., Melendez, F.J. 1999. *J. Mol. Structure (Theochem),* 493: 171.

Prasad, P.N., Williams, D.J. 1991. Introduction to nonlinear optical effects in molecules and polymers. Wiley, New York.

Premkumar, S., Jawahar, A., Mathavan, T., Kumara Dhas, M., Milton Franklin Benial, A. 2015 *SpectrochimicaActa Part A: Mol. Biomol. Spect.,* 138: 252–263.

Pulay, P., Fogarasi, G., Pongor, G., Boggs, J.E., Vargha, A. 1983. *J. Am. Chem. Soc.,* 105: 7037–7047.

Pulay, P., Forgarasi, G., Pong, F., Boggs, J.E. 1979. *J. Am. Chem. Soc.,* 101: 2550–2560.

Rajeev T. Ulahannan, YohannanPanicker, C., HemaTresa Varghese, C., Van Alsenoy, Robert Musiol and Josef Jampilek, P.L. Anto, *SpectrochimicaActa Part A: Mol. Biomol. Spect.*, 121: 445–456.

Raschi, A.B., Romano, E. 2010. *Spectrochim. Acta A,* 77: 497–505.

Rauhut, G., Pulay, P. 1995. *J. Phys. Chem.*, 99: 3093–3100.

Ravikumar, C., Padmaja, L., Hubert Joe, I. 2010. *Spectrochim.Acta A.,* 75: 859–866.

Reed, A.E., Curtiss, L.A., Weinhold, F. 1988. *Chem. Rev.,* 88: 899–926.

Sathyanarayana, D.N. 1996. Vibrational spectroscopy theory and application. New Age International Publishers, New Delhi.

Schlegel, H.B. 1982. *J. Comput. Chem.,* 3: 214–218.

Scrocco, E., Tomasi, J. 1978. *Adv. Quantum Chem.*, 11: 115.

Sebastian, S., Sylvestre, S., Sundaraganesan, N., Amalanathan, M., Ayyapan, S., Oudayakumar, K., Karthikeyan, B. 2013.*SpectrochimicaActa Part A: Mol. Biomol. Spect.*, 107: 167–178.

Sheena Mary, Y., YohannanPanicker, C., HemaTresa Varghese, K. Raju, TugbaErtanBolelli, IlkayYildiz, Carlos M. Granadeiro, Helena I.S. Nogueira, 2011. *J. Mol. Struct.,* 994: 223–231.

Shobaa, D., Periandy, S., Karabacak, M., Ramalingam, S. 2011. *Spectrochim. Acta Part A,* 83: 540–552.

ShrutiMaheshwary, U., Lourderaj, N. Sathyamurthy, 2006. *J. Phys. Chem. A.*, 110: 12662–12669.

Sullivan, C., Sherma, J. 2006. *ActaChromatogr.*, 16: 153–163

Sundaraganesan, N., Dominic Joshua, B., Meganathan, C., Meenashi, R., Cornard, J.P. 2008. *Spectrochim. Acta Part A.,* 70: 376–383.

Sundius, T. 1990. MOLVIB: a program for harmonic force felds calculations, CPE Program No. 604, *J. Mol. Struct.,* 218: 321–326.

Sundius, T. 2002. MOLVIB (v.7.0); calculation of harmonic force fields and vibrational modes of molecules, QCPE, Program No. 807.

Sundius, T. 2002. *Vib. Spectrosc.,* 29: 89–95.

Szafran, M., Komasa, A., Adamska, E.B., *J. Mol. Struct. (THEOCHEM),* 827: 101–107.

Takeuchi, H., Sato, M., Tsuji, T., Takashima, H., Egawa, T., Konaka, S. 1999. *J. Mol. Struct.,* 485–486: 175–181.

Yaping Tao, Ligang Han, Yunxia Han and Zhaojun Liu, *SpectrochimicaActa Part A: Mol. Biomol. Spect.*, 137: 1078–1085.

Yifan Jin, Yanyan Zhu, Mingsheng Tang, 2011. *Comp. Theo. Chem.,* 963: 268–272.

Yu Zhang, Fang Zhang, Kuirong Ma and Guodong Tang, 2013. *SpectrochimicaActa Part A: Mol. Biomol. Spect.*, 105: 352–358.

Zeegers, T., Hyskens, P., Hyskens, 1991. intermolecular forces- An introduction to modern methods and results, Springer-Verlag, Berlin.